Journal of Earthquake Engineering

ISSN: (Print) (Online) Journal homepage: www.tandfonline.com/journals/ueqe20

Pseudo-Velocity Response Spectrum to Velocity Response Spectrum Conversion Model

Zheng Liu, Yan-Gang Zhao & Haizhong Zhang

To cite this article: Zheng Liu, Yan-Gang Zhao & Haizhong Zhang (07 Mar 2024): Pseudo-Velocity Response Spectrum to Velocity Response Spectrum Conversion Model, Journal of Earthquake Engineering, DOI: 10.1080/13632469.2024.2323986

To link to this article: https://doi.org/10.1080/13632469.2024.2323986

Published online: 07 Mar 2024.

JOURNAL OF EARTHQUAKE ENGINEERING
https://doi.org/10.1080/13632469.2024.2323986

Pseudo-Velocity Response Spectrum to Velocity Response Spectrum Conversion Model

Zheng Liu[a], Yan-Gang Zhao[a], and Haizhong Zhang[b]

[a]Key Laboratory of Urban Security and Disaster Engineering of Ministry of Education, Beijing University of Technology, Beijing, China; [b]Eco-Science Course, Faculty of Agriculture, Yamagata University, Yamagata, Japan

ABSTRACT

Velocity response spectrum (SV) plays a critical role in the seismic design of structures equipped with velocity-dependent dampers. Often, the SV is approximated using the pseudo-velocity response spectrum (PSV), because of the lack of information on the SV in seismic codes. As indicated in the existing literature, the error of this approximation is significant for short and long periods, and therefore, researchers have started to develop PSV to SV conversion models for obtaining SV more accurately. Recent studies discovered that the relationship between the PSV and SV is affected not only by structural parameters, but also by magnitude, distance, and site class. However, models for converting PSV to SV including magnitude, distance, and site class as input parameters have not been developed. To this end, a PSV to SV conversion model including magnitude, distance, and site class is proposed in this study based on a large number of real ground motion records (16,660 horizontal acceleration time histories) selected from the Japan Strong Motion Network. Furthermore, since the magnitude and distance are not specified in the seismic design, a response-spectrum-shape factor, *s*, is discussed to reflect the influences of magnitude and distance. Accordingly, an *SV/PSV* model incorporating *s* is established. The proposed models show better accuracy than the existing models for cases with different magnitudes, distances, and site classes.

ARTICLE HISTORY
Received 25 May 2023
Accepted 22 February 2024

KEYWORDS
Velocity response spectrum; pseudo-velocity response spectrum; magnitude; distance; site class

1. Introduction

The velocity response spectrum (SV) is necessary for calculating the relative peak velocities at both ends of the damper and determining the design force (FEMA-450 2003) in the seismic design of structures equipped with velocity-dependent dampers. SV is often approximated using the pseudo-velocity response spectrum (PSV) because it is not specified in most seismic codes; PSV can be converted from the pseudo-acceleration response spectrum (PSA) defined in the seismic codes (Gupta and Trifunac 1990; Kumari and Gupta 2007; Sadhu and Gupta 2008; Trifunac and Gupta 1991). However, Sadek et al. (2000) indicated that this approximation is only valid in mid-periods, and the PSV is significantly larger than SV in short periods, and it is smaller than SV in long periods.

Thus far, several studies have focused on developing PSV to SV conversion models. Sadek et al. (2000) established an *SV*/*PSV* model by analyzing 72 horizontal components of accelerograms from 36 stations in the western United States. This model takes into account the influences of the damping ratio and structural period. Desai and Tande (2018) also established an *SV*/*PSV* model by analyzing an ensemble of 108 strong ground motions in the United States; this model also takes into account the influences of the damping ratio and structural period.

Many subsequent studies (Desai and Tande 2017; Gupta 2009; Pal and Gupta 2021; Samdaria and Gupta 2018) reported that the validity of using PSV to approximate SV was affected not only by the

CONTACT Haizhong Zhang zhang@tds1.tr.yamagata-u.ac.jp Eco-Science Course, Faculty of Agriculture, Yamagata University, 1-23, Wakaba-machi, Tsuruoka-shi, Yamagata 997-8555, Japan

damping ratio and period but also by the ground-motion characteristics. Gupta (2009) indicated that the frequency components of ground motion affect the relationship between SV and PSV over short periods. Therefore, he established a PSV to SV conversion model for short periods, incorporating the mean period corresponding to the centroid of the ground-motion Fourier spectrum, based on random vibration theory. Desai and Tande (2017) further developed a PSV to SV conversion model for long periods (>0.86 s) based on Gupta's model (Gupta 2009). Their model incorporates a period corresponding to the centroid of the displacement response spectrum (SD). Samdaria and Gupta (2018) also established a PSV to SV conversion model applicable to longer periods (up to 15 s); this model considers the effect of the period corresponding to the maximum value of PSV and the decline rate of PSA over long periods. Pal and Gupta (2021) improved Gupta's model (Gupta 2009) over short periods. In addition, Santos-Santiago et al. (2022) established an *SV*/*PSV* model based on 1272 ground motions recorded at 79 seismic stations in Mexico; this model includes the dominant period of PSA corresponding to the eight zones defined by Castillo and Ruiz (2014).

The above-mentioned research studies focused on the influence of ground motion characteristics on the relationship between the SV and PSV. In reality, these characteristics of ground motion are essentially determined by seismic parameters; such as magnitude, distance, and site class (Andreotti and Calvi 2021; Calvi and Andreotti 2022; Zhang and Zhao 2021; Zuccolo, Andreotti, and Calvi 2023). Papagiannopoulos et al. (2013) and Zhang and Zhao (2021) systematically analyzed the effects of these three seismic parameters on the relationship between PSV and SV. However, a PSV to SV conversion model directly including magnitude, distance, and site class as input parameters has not been developed.

The purpose of this study is to propose a PSV to SV conversion model considering the effects of magnitude, distance, and site class, which can also be directly used for seismic design. The rest of the paper is as follows. The second section reviews existing PSV to SV conversion models. The third section discusses the influences of magnitude, distance, and site class on the PSV-SV relationship using a large number of earthquake records (16660 earthquake acceleration time histories) selected from the strong motion network in Japan. The fourth section proposes a PSV to SV conversion model, considering the influence of these three seismic parameters, and compares it with existing models. The final section shows the conclusions.

2. Literature Review

Sadek et al. (2000) established an *SV*/*PSV* model by analyzing 72 horizontal components of accelerograms from 36 stations in the western United States. This model was proposed considering a period range of 0.1 s to 4 s and damping ratios from 2% to 60%, which is expressed as

$$\frac{SV}{PSV}=\left(1.095+0.647\xi-0.382\xi^2\right)T^{(0.193+0.838\xi-0.621\xi^2)} \tag{1}$$

where ξ and T are the damping ratio and the natural structural period, respectively. All symbols and abbreviations are detailed in Appendix A.

Desai and Tande (2018) also established an *SV*/*PSV* model by analyzing an ensemble of 108 strong ground motions in the United States. This model is proposed considering a period range from 0 s to 4 s and damping ratios from 5% to 99%, which is expressed as

$$\frac{SV}{PSV}=1+q_1q_2q_3T^{q_3+q_4-1} \tag{2}$$

where $q_1 - q_4$ are regression coefficients, which are expressed as

$$q_1=0.9738+0.05634\xi-0.049\xi^{0.2535} \tag{2a}$$

$$q_2=0.9058+0.1387\xi-0.27\xi^{0.1388} \tag{2b}$$

$$q_3 = 0.0702 + 0.4472\sqrt{\xi} \tag{2c}$$

$$q_4 = \frac{0.5989 + 1.162\xi}{0.3122 + \xi} \tag{2d}$$

Gupta (2009) established a PSV to SV conversion model suitable for short periods using random vibration theory. This model is suitable for cases in which the period is less than the mean period (T_c) of the base acceleration corresponding to the centroid of its Fourier spectrum, and the damping ratio is less than 10%. This model is expressed as

$$SV = \frac{T}{2\pi}\sqrt{PSA^2 - PGA^2}, T < T_c \tag{3}$$

where PGA is the peak ground acceleration, and T_c is defined as (Rathje et al. 2004)

$$T_c = \frac{\sum_n \frac{C_n^2}{f_n}}{\sum_n C_n^2} \tag{3a}$$

where C_n is Fourier amplitudes of ground motion at discrete frequencies f_n between 0.25 Hz and 20 Hz.

Further, Desai and Tande (2017) established a PSV to SV conversion model suitable for long periods (>0.86 s) based on Gupta's model (Gupta 2009) by analyzing 172 ground motions. This model was proposed considering a period range of 0.86 s to 4 s and a damping ratio of 5%, which is expressed as

$$SV = \begin{cases} \frac{T}{2\pi}\sqrt{PSA^2 - PGA^2} & T < T_c \\ \frac{T}{2\pi}PSA & T_c \leq T \leq 0.86\text{s} \\ 1 + 10^{-1.7914\bar{T}+3.5461}(T - 0.86) & T \geq 0.86\text{s} \end{cases} \tag{4}$$

where $\bar{T}$ is the period corresponding to the centroid of the spectral displacement (SD) curve.

Samdaria and Gupta (2018) also established a PSV to SV conversion model for long periods (up to 15 s) by analyzing SV/PSV values; this model was proposed considering periods of less than 15 s and damping ratios from 0% to 10%, which are expressed as

$$SV = \begin{cases} \frac{T}{2\pi}\sqrt{PSA^2 - PGA^2} & T < T_c \\ \frac{T}{2\pi}PSA & T_c \leq T \leq T_{\max} \\ \frac{T}{2\pi}PSA\left(\frac{T}{T_{\max}}\right)^l & T \geq T_{\max} \end{cases} \tag{5}$$

where $T_{\max}$ represents the end of the velocity-sensitive region in the response spectrum, and l represents the change speed of the PSV deviating from the SV as T increases; they are expressed as

$$T_{\max} = o_1 + o_2 T_{PSV} \tag{5a}$$

$$l = o_3 + o_4 p \tag{5b}$$

where o_1–o_4 are regression coefficients which can be obtained from Table 1 of Samdaria and Gupta (2018). The coefficient p is defined as

$$p = \frac{\log PSA(T_{\text{end}}) - \log PSA(T_{\max})}{\log T_{\text{end}} - \log T_{\max}} \tag{5c}$$

where T_{end} is the longest period of PSA, $PSA(T_{\text{end}})$ is the value of PSA corresponding to the period T_{end}, and $PSA(T_{\max})$ is the value of PSA corresponding to the period $T_{\max}$.

Pal and Gupta (2021) further improved Gupta's model (Gupta 2009) over short periods. This improved model applies to a period range of 0 s to 15 s and damping ratios from 0% to 10%, which is expressed as

$$SV = \begin{cases} C(T)\frac{T}{2\pi}\sqrt{PSA^2 - PGA^2} & T < T_{\lim} \\ \frac{T}{2\pi}PSA & T_{\lim} \le T \le T_{\max} \\ \frac{T}{2\pi}PSA\left(\frac{T}{T_{\max}}\right)^l & T \ge T_{\max} \end{cases} \tag{6}$$

where $C(T)$ is the transition curve of the short periods, $T_{\lim}$ is a limiting period significantly longer than T_c, they are expressed as

$$T_{\lim} = \begin{cases} w_0 T_{PSA} + w_1 & T_{PSV} \le 0.5s \\ w_2 + w_3(T_{PSV})^{-1} & 0.5 < T_{PSV} \le 1.0s \\ w_4 T_{PSA} + w_5 T_{PSV} + w_6 & T_{PSV} > 1.0s \end{cases} \tag{6a}$$

$$C(T) = 1 + (r-1)\left(\frac{T}{T_{\lim}}\right)^5 \tag{6b}$$

where w_0 – w_6 are regression coefficients, T_{PSA} represents the period when the PSA reaches its maximum value, and T_{PSV} represents the period when the PSA value reaches the maximum. In Eq. (6b), the coefficient r is defined as

$$r = \sqrt{\frac{PSA_{\lim}^2}{PSA_{\lim}^2 - PGA^2}} \tag{6c}$$

where $PSA_{\lim}$ denotes the value of PSA corresponding to the period $T_{\lim}$.

Santos-Santiago et al. (2022) established an SV/PSV model based on 1272 ground motions recorded at 79 seismic stations in Mexico City. This model was proposed considering a period range of 0.1 s to 6 s and applies to damping ratios from 5% to 30%; it is expressed as

$$\frac{SV(T,\xi)}{PSV(T,\xi)} = (u_1\xi + u_2)T^{(u_3\xi + u_4)} \tag{7}$$

where, u_1 – u_4 are the regression coefficients related to the dominant period (T_s), which is recognized as the period when the PSA is the maximum. The values of u_1 – u_4 belonging to zone A to zone H of Mexico City (Castillo and Ruiz 2014) classified by T_s are listed in Table 3 of Santos-Santiago et al. (2022).

Papagiannopoulos et al. (2013) found that the relationship between PSV and SV is not only affected by the structural parameters but also by magnitude, distance, and site class. Therefore, they established a conversion model from PSV to SV based on 866 selected accelerograms from various earthquakes recorded worldwide. The model is proposed taking into account the period range of 0 s to 5 s and is applicable for damping ratios of 5% to 50%, which are expressed as

$$\frac{SV(T,\xi)}{PSV(T,\xi)} = k_1 + k_2T + k_3\xi + k_4T^2 + k_5\xi^2 + k_6T\xi \tag{8}$$

$$\frac{SV(T,\xi)}{PSV(T,5\%)} = k_7 + k_8T + k_9\ln\xi + k_{10}T^2 + k_{11}(\ln\xi)^2 + k_{12}T\ln\xi \tag{9}$$

where k_1–k_{12} are regression coefficients, which are listed in Tables 6 and 8 of Papagiannopoulos et al. (2013).

However, a PSV to SV conversion model directly including magnitude, distance, and site class as input parameters has not been developed. The purpose of this study is to propose a PSV to SV conversion model considering the effects of magnitude, distance, and site class, which can also be directly used for seismic design.

3. Effects of Magnitude, Distance, and Site Class on *SV/PSV*

3.1. Database

To explore the effects of magnitude, distance, and site class on *SV/PSV*, and propose an *SV/PSV* model considering these effects, a total of 16,660 horizontal acceleration time histories are collected from the strong-motion seismograph networks, K-NET, KiK-net (Aoi et al. 2011; Hang et al. 2022; Okada et al. 2004; Zhang, Zhao et al. 2023), which were constructed by the National Research Institute for Earth Science and Disaster Resilience (1995). The PGA of each record is selected to be greater than 20 gal to increase the signal-to-noise ratio and minimize the impact of noise. These acceleration time histories are recorded at 338 stations with magnitudes (M) of 4–9 and epicenter distances (R) of 10–200 km. Further, these sites are categorized into four site classes to explore site effects: B, C, D, and E, according to the average shear-wave velocity in the upper 30 m ($\bar{v}_{s30}$) specified by the National Earthquake Hazards Reduction Program (2000). This paper does not include site class A, because there are few sites belonging to this site class in K-NET and KiK-net. In addition, the hypocenter depth of the chosen seismic data ranges from 0 km to 196 km (Zhang, Deng et al. 2023). The selected earthquakes include both interplate (e.g. 2003 Tokachi earthquake and 2011 off the Pacific coast of Tohoku earthquake) and intraplate earthquakes (e.g. 2000 Tottori earthquake, 2004 Chuetsu earthquake, 2016 Kumamoto earthquakes, and 2018 Hokkaido Eastern Iburi earthquake). Since rupture depth and style of faulting are not provided in K-NET and KiK-NET, their information is not included in this paper. The shear-wave velocity provided by the KiK-net network is greater than 30 m, and thus, $\bar{v}_{s30}$ can be obtained directly. However, K-NET provides the shear-wave velocity in the upper 20 m ($\bar{v}_{s20}$) only. Here, $\bar{v}_{s30}$ is obtained from $\bar{v}_{s20}$ according to the formula proposed by Kanno et al. (2006)

$$\bar{v}_{s30} = 1.13\bar{v}_{s20} + 19.5 \tag{10}$$

The distributions of magnitude M and distance R for the four classes are shown in Fig. 1.

The collected records in each site class are classified into three groups based on magnitude for exploring the effect of magnitude M on *SV/PSV*: $M \in [4, 5.5)$, $M \in [5.5, 6.5)$, and $M \in [6.5, +\infty)$. Each group is further divided into three subgroups based on the distance to explore its influence: $R \in [10\text{ km}, 50\text{ km})$, $R \in [50\text{ km}, 100\text{ km})$, and $R \in [100\text{ km}, 200\text{ km}]$, as listed in Table 1. In addition, all the selected ground-motion records are consistently processed. A baseline adjustment is applied to all records to remove long-period noise.

3.2. Variation Trend of SV/PSV with Magnitude, Distance, and Site Class

Firstly, the SV and PSV of all selected records are calculated considering structural periods from 0.01 s to 6 s (interval 0.01 s) and damping ratios of 5%, 10%, 20%, 30%, 40%, and 50%. Then, the average value of *SV/PSV* of each group is calculated.

Figures 2 and 3 compare the results of *SV/PSV* with different magnitudes of $R \in [50\text{ km}, 100\text{ km})$ in site classes B and E, respectively. The variation trend of *SV/PSV* with magnitude is different for periods longer and shorter than the value corresponding to *SV/PSV* = 1. The *SV/PSV* changes little with magnitude in short periods, whereas the *SV/PSV* decreases greatly with the magnitude over long periods. The average values of 5%-damped *SV/PSV* in the periods of 0.01–0.1 and 1–6 s are used to quantify the impact of magnitude on *SV/PSV* in short and long periods, respectively. When the magnitude varies from [4, 5.5) to [6.5, +∞), the average value of *SV/PSV* decreases by 82% at 1–6 s, while it changes by only 2% at 0.01–0.1 s for the cases in site class B. The trend of *SV/PSV* value with magnitude did not change with the damping ratio ξ. In addition, it is found that the period corresponding to *SV/PSV* = 1 increased with the magnitude. These conclusions are still valid for the results not shown in Figs. 2 and 3, such as those of site classes C and D, and distances $R \in [10\text{ km}, 50\text{ km})$ and $R \in [100\text{ km}, 200\text{ km}]$.

Figures 4 and 5 compare the results of *SV/PSV* with different distances of $M \in [5.5, 6.5)$ in site classes B and E, respectively. The *SV/PSV* varies slightly with distance. The variation trend of *SV/PSV* with distance is also different at periods longer and shorter than the value corresponding to *SV/PSV* = 1. In

Table 1. Classification of records according to magnitude, distance, and site class.

Group	Record count	Distance R (km)	Magnitude M	Site class
1	1102	$R \in [10, 50)$	$M \in [4, 5.5]$	B
2	700	$R \in [50, 100)$		
3	196	$R \in [100, 200]$		
4	142	$R \in [10, 50)$	$M \in [5.5, 6.5]$	
5	298	$R \in [50, 100)$		
6	274	$R \in [100, 200]$		
7	40	$R \in [10, 50)$	$M \in [6.5, +\infty]$	
8	102	$R \in [50, 100)$		
9	178	$R \in [100, 200]$		
10	1326	$R \in [10, 50)$	$M \in [4, 5.5]$	C
11	978	$R \in [50, 100)$		
12	272	$R \in [100, 200]$		
13	164	$R \in [10, 50)$	$M \in [5.5, 6.5]$	
14	384	$R \in [50, 100)$		
15	470	$R \in [100, 200]$		
16	102	$R \in [10, 50)$	$M \in [6.5, +\infty]$	
17	176	$R \in [50, 100)$		
18	412	$R \in [100, 200]$		
19	1606	$R \in [10, 50)$	$M \in [4, 5.5]$	D
20	1566	$R \in [50, 100)$		
21	706	$R \in [100, 200]$		
22	194	$R \in [10, 50)$	$M \in [5.5, 6.5]$	
23	568	$R \in [50, 100)$		
24	1046	$R \in [100, 200]$		
25	104	$R \in [10, 50)$	$M \in [6.5, +\infty]$	
26	116	$R \in [50, 100)$		
27	512	$R \in [100, 200]$		
28	828	$R \in [10, 50)$	$M \in [4, 5.5]$	E
29	594	$R \in [50, 100)$		
30	206	$R \in [100, 200]$		
31	124	$R \in [10, 50)$	$M \in [5.5, 6.5]$	
32	278	$R \in [50, 100)$		
33	542	$R \in [100, 200]$		
34	38	$R \in [10, 50)$	$M \in [6.5, +\infty]$	
35	68	$R \in [50, 100)$		
36	248	$R \in [100, 200]$		
36	16660			

short periods, the SV/PSV decreases with an increase in distance. In long periods, the SV/PSV increases slightly with an increasing distance in site class B, while the variation degree becomes very small for site class E. For the cases in site class B, when the distance varies from [10 km, 50 km) to [100 km, 200 km], the average value of SV/PSV decreases by 8% at 0.01–0.1 s, while it increases by 29% at 1–6 s. For the cases in site class E, when the distance varies from [10 km, 50 km) to [100 km, 200 km], the average value of SV/PSV decreases by 18% at 0.01–0.1 s, while it changes by only 8% at 1–6 s. In addition, it is found that the period corresponding to $SV/PSV = 1$ varied slightly with distance. These conclusions are still valid for the results not shown in Figs. 4 and 5, such as those of site classes C, and D, and magnitudes $M \in [4, 5.5)$ and $M \in [6.5, +\infty)$.

Figures 6–8 compare the results of SV/PSV under different site classes of distances $R \in [50\ \text{km}, 100\ \text{km})$ for magnitudes $M \in [4, 5.5)$, $M \in [5.5, 6.5)$, and $M \in [6.5, +\infty)$, respectively. SV/PSV gradually decreases as the site varies from B to E; however, this trend becomes unobvious for large magnitudes and long periods by comparing Figs. 6–8. For the cases in Fig. 6, when the site class varies from B to E, the average value of SV/PSV decreases by 36% at 0.01–0.1 s, while it decreases by 52% at 1–6 s. For the cases in Fig. 8, when the site class varies from B to E, the average value of SV/PSV decreases by 55% at 0.01–0.1 s, while it decreases by 28% at 1–6 s. In addition, it is found that the period corresponding to $SV/PSV = 1$ increased as the site class varied from B to E. The same phenomenon is observed for the results not shown here, such as those of distances $R \in [10\ \text{km}, 50\ \text{km})$ and $R \in [100\ \text{km}, 200\ \text{km}]$.

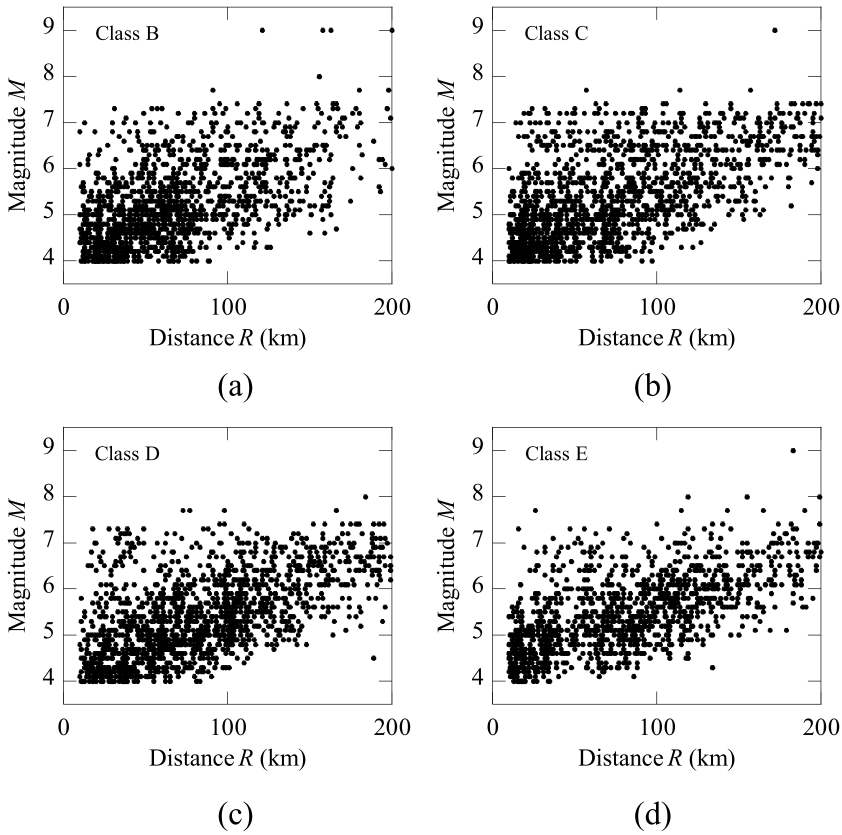

Figure 1. Distribution of magnitude M and distance R.

Figures 9 and 10 investigate the variation of SV/PSV with damping ratios. For this purpose, Fig. 9a,b superimpose the mean of three magnitude graphs considered under each damping ratio in Figs. 2 and 3, respectively. Similarly, Fig. 10a,b superimpose the mean of the three distance graphs considered under each damping ratio in Figs. 4 and 5, respectively. It can be found that SV/PSV increases with the damping ratio at long periods but decreases at the majority of short periods, which is consistent with those observed in previous studies. However, the average value of SV/PSV becomes close between any two distinct dampings, as the damping increases beyond 30%. Similar trends were observed for other distance ranges and magnitude ranges.

The physical reasons for the variation trend of SV/PSV with magnitude and distance may be attributed to the different attenuation manner of SV and PSV with magnitude and distance. Maybe, SV increases more slowly than PSV with increasing magnitude, particularly at long periods. Although this point has never been discussed in previous studies, Zuccolo et al. (2023) have pointed out the different decay manners of acceleration response spectrum (SA) and displacement response spectrum (SD) with magnitude and distance. This conclusion needs further support in future studies. In addition, the theoretical explanation of the influence of magnitude, distance, and site classes on the trend of SV/PSV variation has been systematically discussed by Zhang and Zhao (2021) based on random vibration theory. Zhang and Zhao (2021) indicated that the variation trend of SV/PSV with the period is mainly controlled by the shape of FAS. Due to the variation of ground motion FAS with magnitude, distance, site class, and damping ratios, the corresponding SV/PSV also changes accordingly with these parameters. The phenomenon explained by Zhang and Zhao (2021) is consistent with the phenomenon described in this paper.

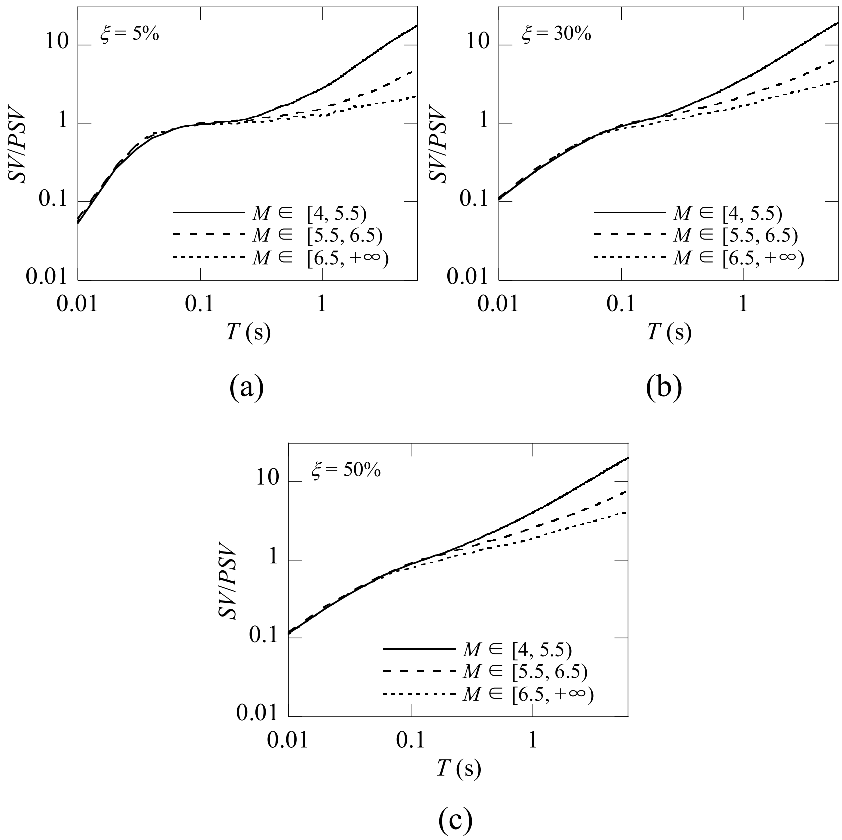

Figure 2. *SV/PSV* with different magnitudes in Class B.

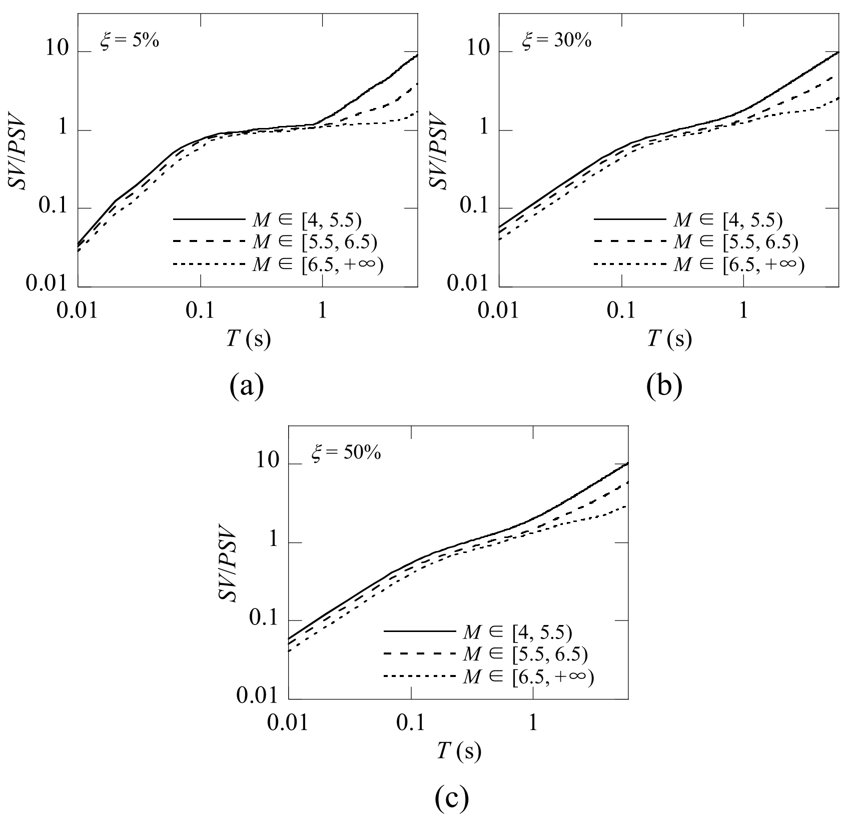

Figure 3. *SV/PSV* with different magnitudes in Class E.

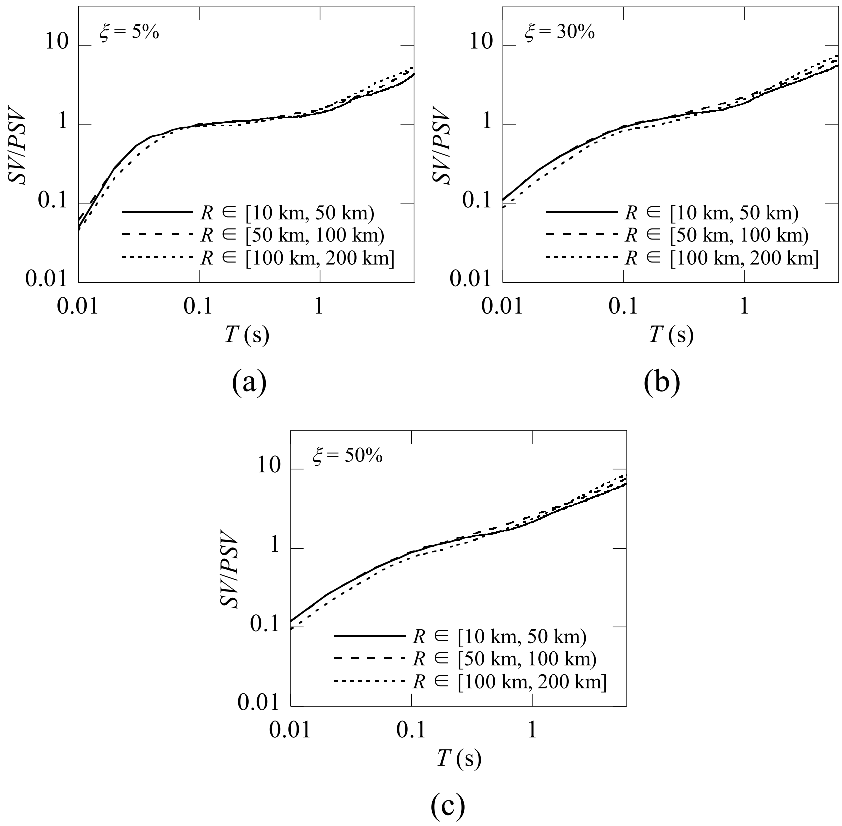

Figure 4. *SV/PSV* with different distances in Class B.

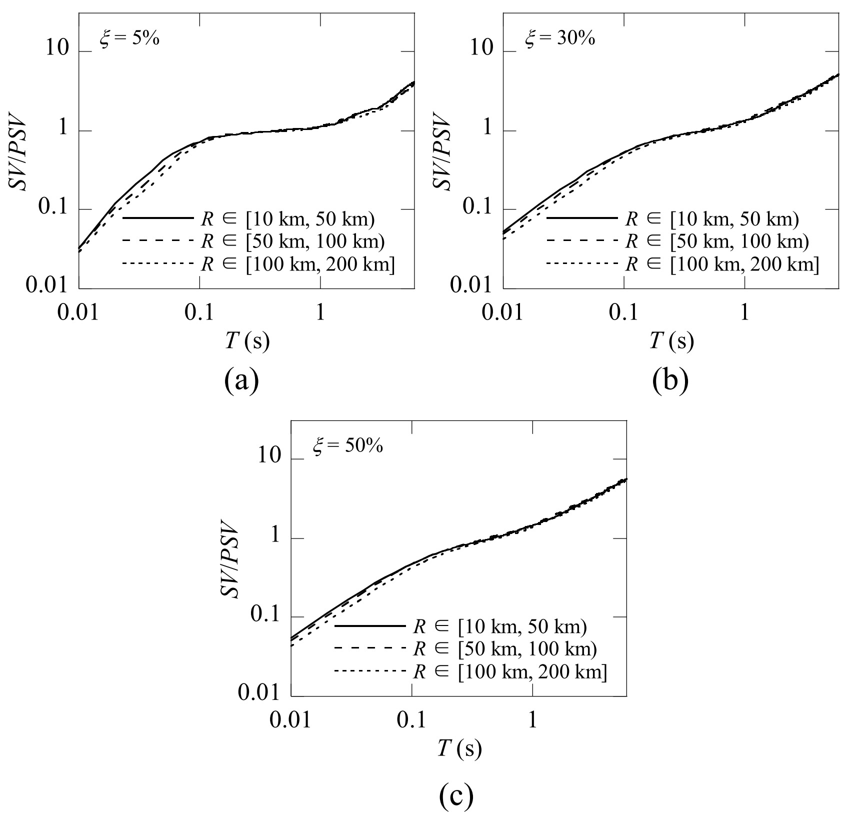

Figure 5. *SV/PSV* with different distances in Class E.

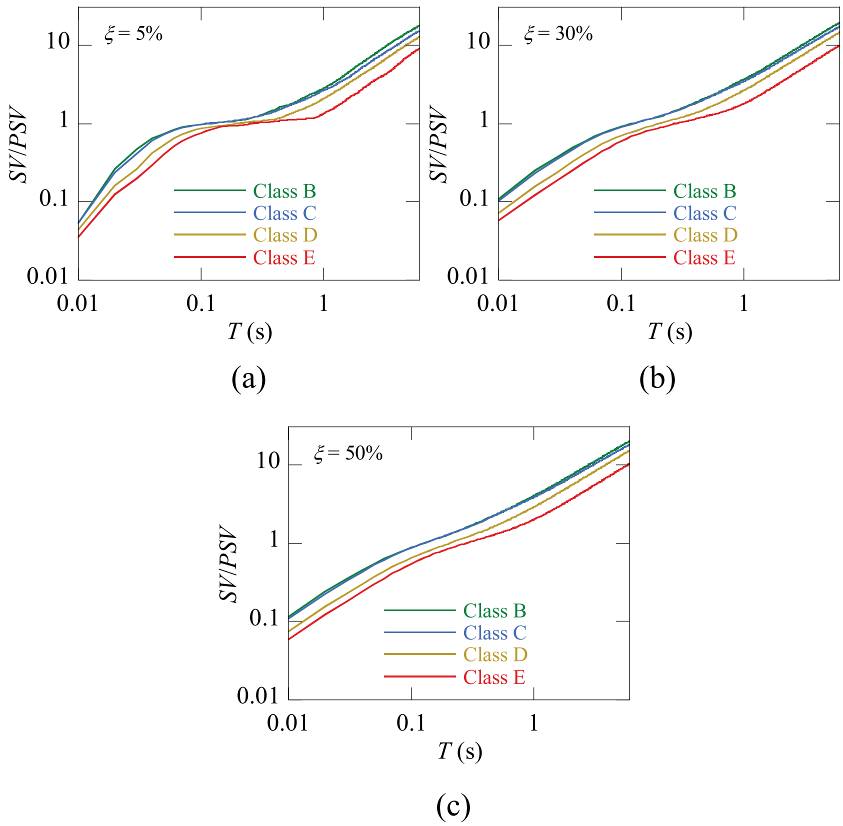

Figure 6. *SV/PSV* in different site classes for magnitudes of $M \in [4, 5.5]$.

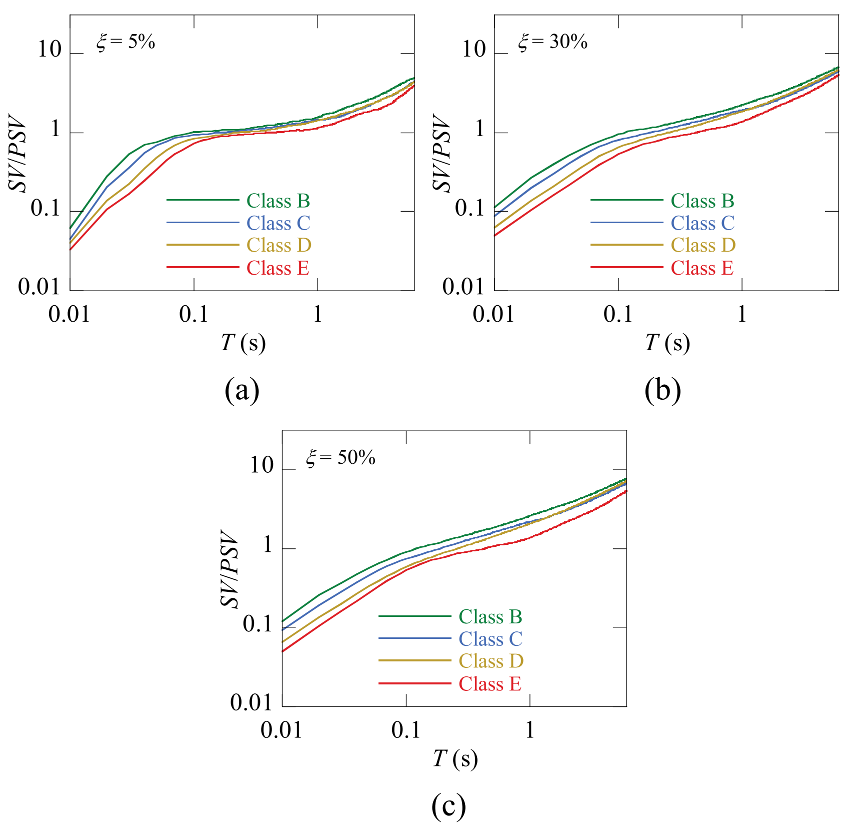

Figure 7. *SV/PSV* in different site classes for magnitudes of $M \in [5.5, 6.5]$.

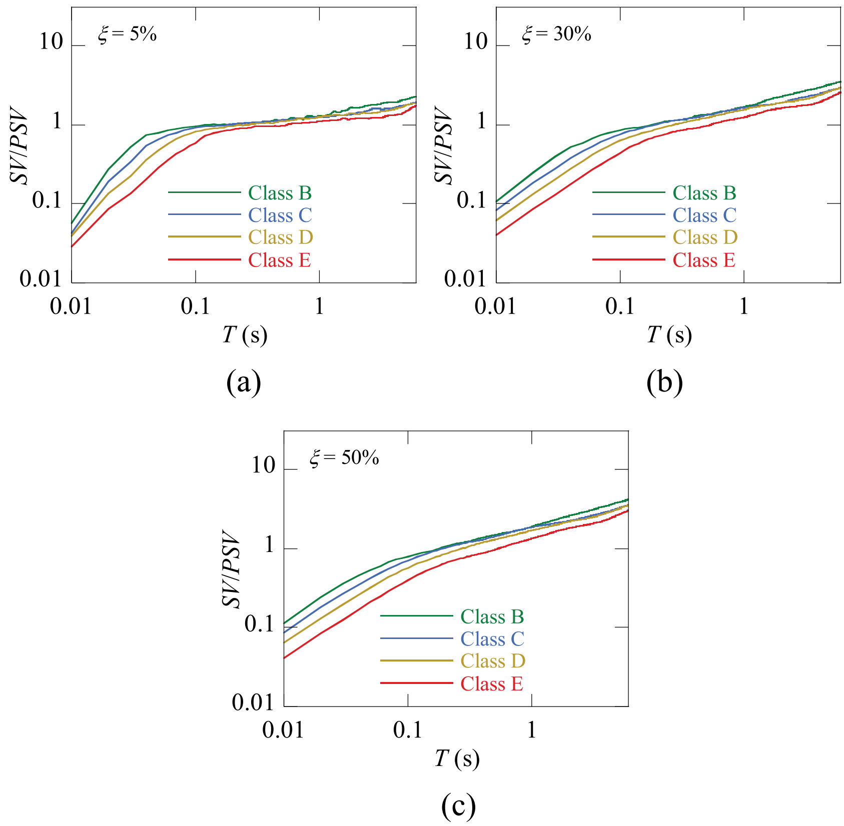

Figure 8. *SV/PSV* in different site classes for magnitudes of $M \in [6.5, +\infty]$.

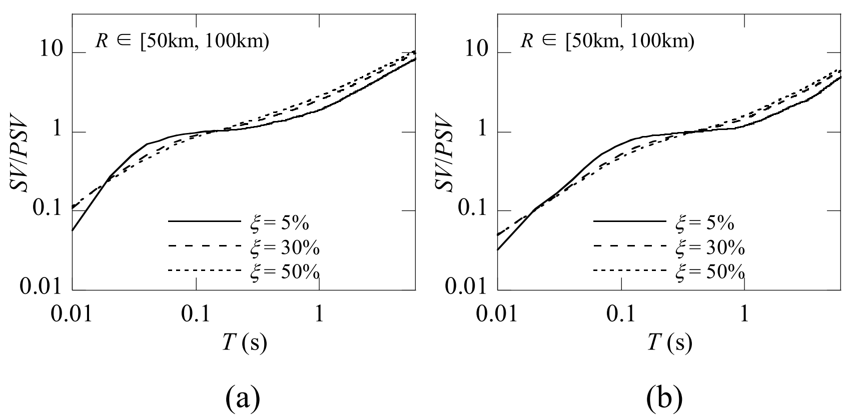

Figure 9. Effect of damping on *SV/PSV* for given distance range. (a) site Class B, (b) site Class E.

4. Proposed *SV/PSV* Model

4.1. Construction of *SV/PSV* Model

Since the variation trends of SV/PSV with the magnitude and distance are different at periods longer and shorter than the value corresponding to $SV/PSV = 1$; the SV/PSV model is regressed as two parts, with the period corresponding to $SV/PSV = 1$ being the demarcation point T_0. Then, an SV/PSV model is proposed by trying a large number of functional forms; this model is expressed as

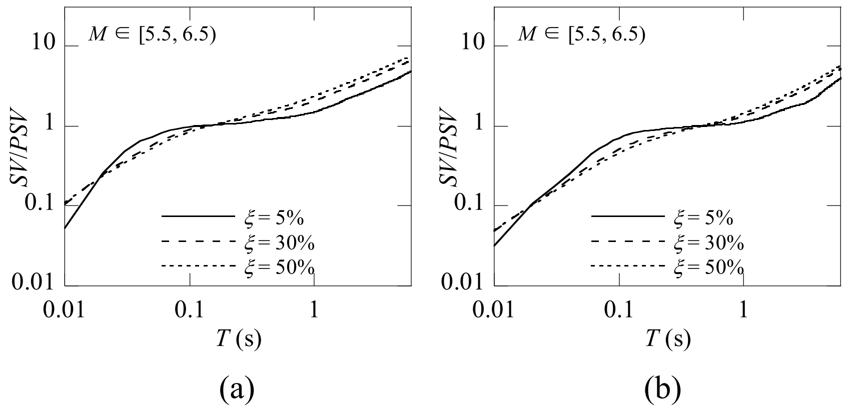

Figure 10. Effect of damping on *SV*/*PSV* for given magnitude range. (a) site Class B, (b) site Class E.

$$\frac{SV}{PSV} = \begin{cases} \left(\frac{T}{T_0}\right)^{(a_1 T + a_2)} & T \le T_0 \\ \left(\frac{a_3}{T^{a_4}}\right)^{(T - T_0)} & T > T_0 \end{cases} \tag{11}$$

where, a_1 — a_4 are regression coefficients. It can be known from Eq. (11) that, when $T = T_0$, $SV/PSV = 1$, when $T < T_0$, $SV/PSV < 1$, when T decreases to zero, SV/PSV approaches zero, and when $T > T_0$, $SV/PSV > 1$, the proposed model satisfies the boundary conditions.

Since T_0 varies with magnitude, distance, and site class, T_0 is regressed as a function of magnitude M, distance R, and site class as

$$T_0 = n_1 e^{(m_1 + m_2 \ln(R) + m_3 M)^{n_2}} \tag{12}$$

where m_1, m_2, m_3, n_1, and n_2 are coefficients regressed nonlinearly based on the least squares method, as indicated in Table 2.

It is found that the coefficients a_1 — a_4 in Eq. (11) are affected by the magnitude, distance, site class, and damping ratio, and their expressions are developed as

$$a_1 = \frac{1}{b_1 + \frac{b_2}{\ln(\xi)} + b_3 e^{(m_1 + m_2 \ln(R) + m_3 M)^{0.5}} (m_1 + m_2 \ln(R) + m_3 M)} \tag{13}$$

$$a_2 = c_1 + \frac{c_2}{\xi^{0.5}} + c_3 (m_1 + m_2 \ln(R) + m_3 M) \tag{14}$$

$$a_3 = d_1 + d_2 \xi^{0.5} + \frac{d_3}{e^{(m_1 + m_2 \ln(R) + m_3 M)^{0.5}}} \tag{15}$$

Table 2. Values of regression coefficients in Eq. (12).

	B	C	D	E
m_1	−12.72	−12.34	−11.67	−11.14
m_2	−0.2584	−0.3598	−0.2932	−0.154
m_3	1.438	1.51	1.405	1.322
n_1	0.27	0.353	0.544	1.308
n_2	0.12	0.135	0.167	0.2754

Table 3. Values of regression coefficients in Eqs. (13–16).

	B	C	D	E
b_1	0.01556	0.04903	0.0798	0.8861
b_2	0.2053	0.2336	0.3558	0.402
b_3	0.2039	0.3643	0.5326	2.642
c_1	0.4192	0.5692	0.527	0.3366
c_2	−0.007749	−0.0185	−0.02765	−0.04541
c_3	−0.06718	−0.04731	−0.05523	−0.09276
d_1	0.641606	0.573863	3.71E−01	0.534294
d_2	0.75224423	0.760537	1.19E + 00	1.051774
d_3	0.073238	0.080006	0.104102	0.095471
e_1	−0.02449	−0.06537	−0.10545	−0.1174
e_2	0.15440286	0.161422	0.277384	0.2857
e_3	0.010591	0.01285	0.016687	0.01677

$$a_4 = e_1 + e_2\xi^{0.5} + \frac{e_3}{e^{(m_1+m_2\ln(R)+m_3M)^{0.5}}} \tag{16}$$

where b_1, b_2, b_3, c_1, c_2, c_3, d_1, d_2, d_3, e_1, e_2, and e_3 are coefficients regressed nonlinearly based on the least squares method, as listed in Table 3.

Figures 11–13 compare the *SV*/*PSV* results obtained using the proposed model with those of the seismic records for damping ratios of 5%, 30%, and 50%, respectively. It can be found that the *SV*/*PSV* results obtained using the proposed model can have high accuracy to keep consistent with those of the

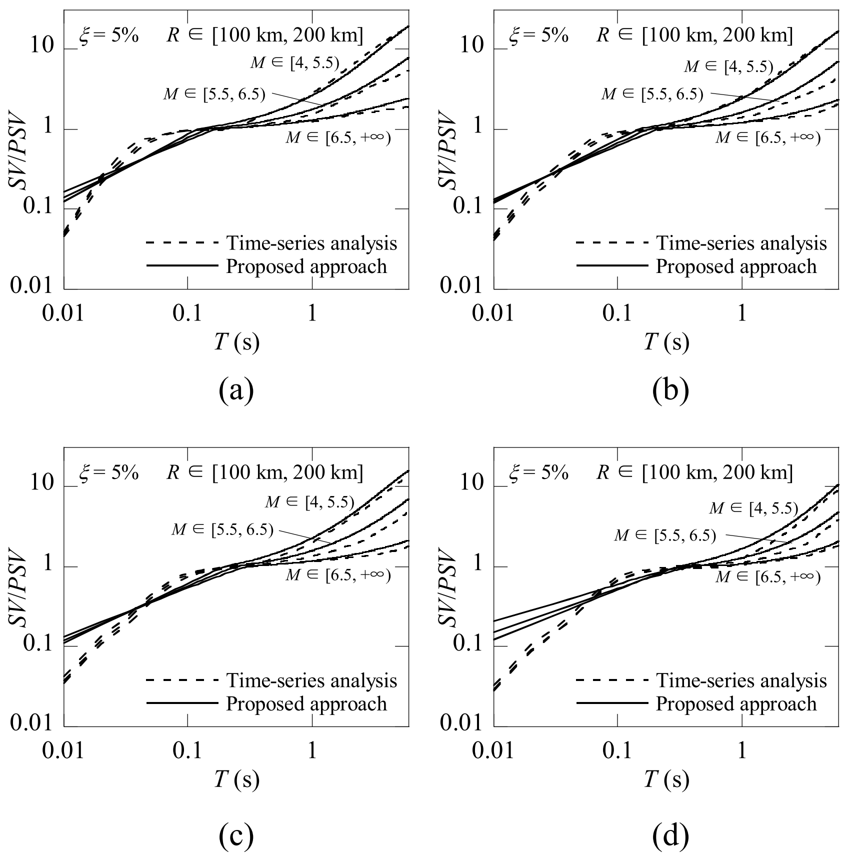

Figure 11. Comparison of the *SV*/*PSV* results obtained by the proposed model and those of ground motion records considering a damping ratio of 5% for (a) Class B, (b) Class C, (c) Class D, (d) Class E.

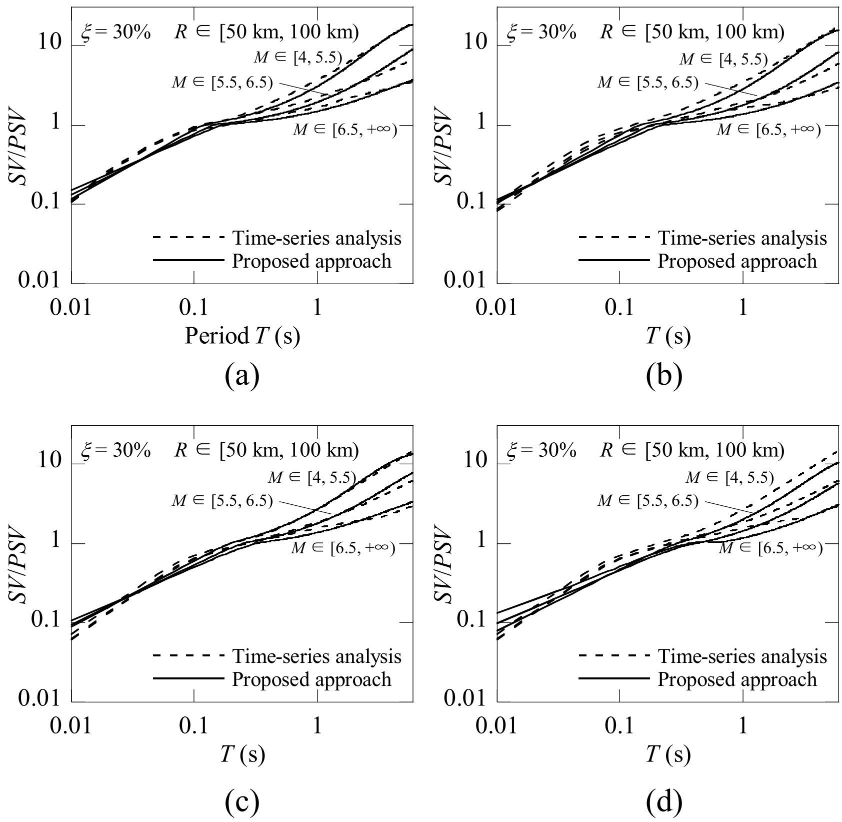

Figure 12. Comparison of the *SV/PSV* results obtained by the proposed model and those of ground motion records considering a damping ratio of 30% for (a) Class B, (b) Class C, (c) Class D, (d) Class E.

seismic records. Moreover, the consistency with the proposed model increases with the increase of the damping ratio in short periods. Similar trends are observed for the results not shown here, such as those of damping ratios 10%, 20%, and 40%.

4.2. Parameter Reflecting the Effects of Magnitude and Distance

Since the magnitude and distance are not specified in the seismic design, it is important to seek out a parameter that can reflect the effect of magnitude and distance, and it can be obtained from the seismic design. Zhang and Zhao (2021) found that magnitude and distance affect the relationship between the PSV and SV by changing the shape of the spectrum. Zhang and Zhao (2022) proposed a response spectrum shape factor s to reflect on the effects of magnitude and distance, which can be obtained from the PSA and expressed as

$$s = \frac{PSA(6s)}{PGA} \tag{17}$$

where $PSA(6s)$ is the value of PSA at 6 s.

Figure 14 depicts the relationship between $\ln(s)$ and the magnitude M and distance R in different site classes. The parameter s is closely correlated with the magnitude and distance, and the $\ln(s)$ increases with increasing M and R. The variation trend of $\ln(s)$ with the magnitude M is considerably more obvious than that with distance R.

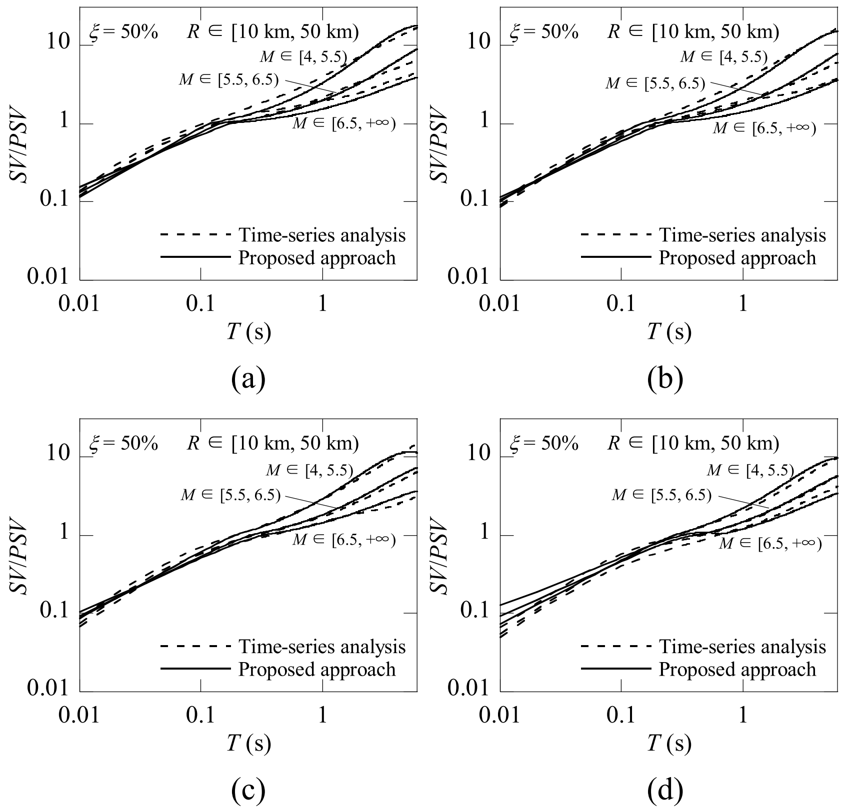

Figure 13. Comparison of the *SV/PSV* results obtained by the proposed model and those of ground motion records considering a damping ratio of 50% for (a) Class B, (b) Class C, (c) Class D, (d) Class E.

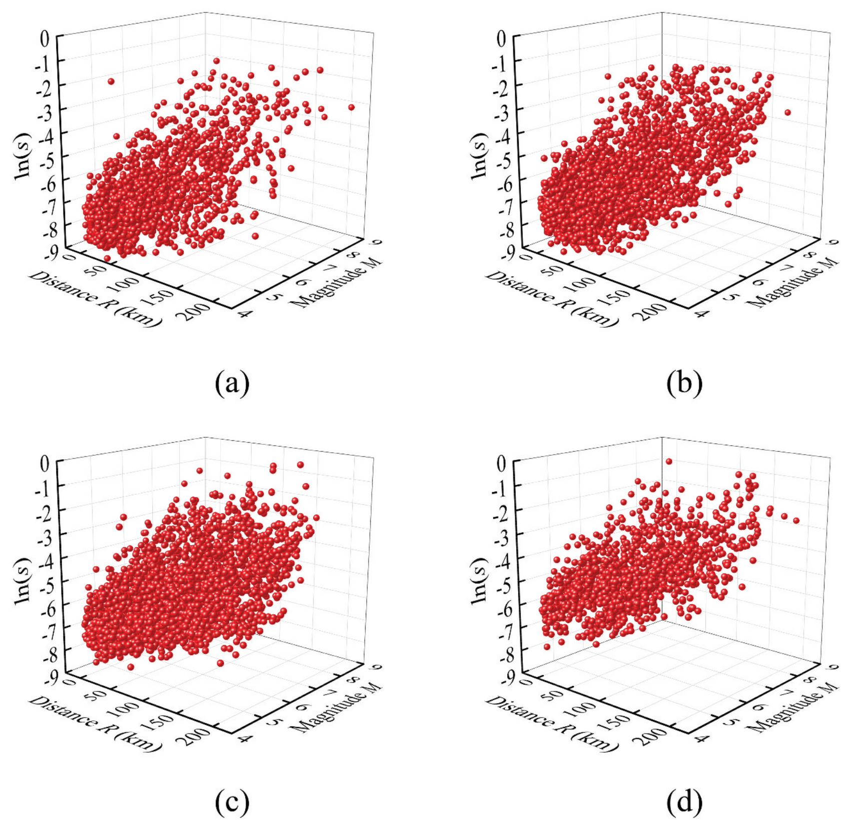

Figure 14. Relationship between ln(s) and the magnitude and distance in different site classes, (a) Class B, (b) Class C, (c) Class D, (d) Class E.

Then, an expression for the relationship between parameter s and magnitude, distance, and site class is regressed as

$$\ln(s) = m_1 + m_2 \ln(R) + m_3 M \tag{18}$$

Then, if Eq. (18) is substituted into Eqs. (12–16), M and R can be replaced by $\ln(s)$. Thus, we can obtain a PSV to SV conversion model that considers the effects of magnitude, distance, and site class and can be directly used for seismic design.

4.3. Comparison of the Results Obtained by the Proposed and Existing Models

The proposed model was compared with existing models, including those of Sadek et al. (2000), Papagiannopoulos et al. (2013), Desai and Tande (2017), Desai and Tande (2018), and Pal and Gupta (2021). Some repressive comparisons of SV/PSV are shown in Figs. 15–26. Figures 15–18 show the results of a 5% damping ratio for site classes B, C, D, and E, respectively. Figures 19–22 show the results of a 10% damping ratio for site classes B, C, D, and E, respectively. Figures 23–26 show the results of a 20% damping ratio for site classes B, C, D, and E, respectively. Figures 19–22 do not include the results of the Desai and Tande model (Desai and Tande 2017) because it does not apply to cases in which the damping ratio is larger than 5%. Figures 23–26 do not include the results of the Pal and Gupta model (Pal and Gupta 2021) because it does not apply to cases in which the damping ratio is larger than 10%.

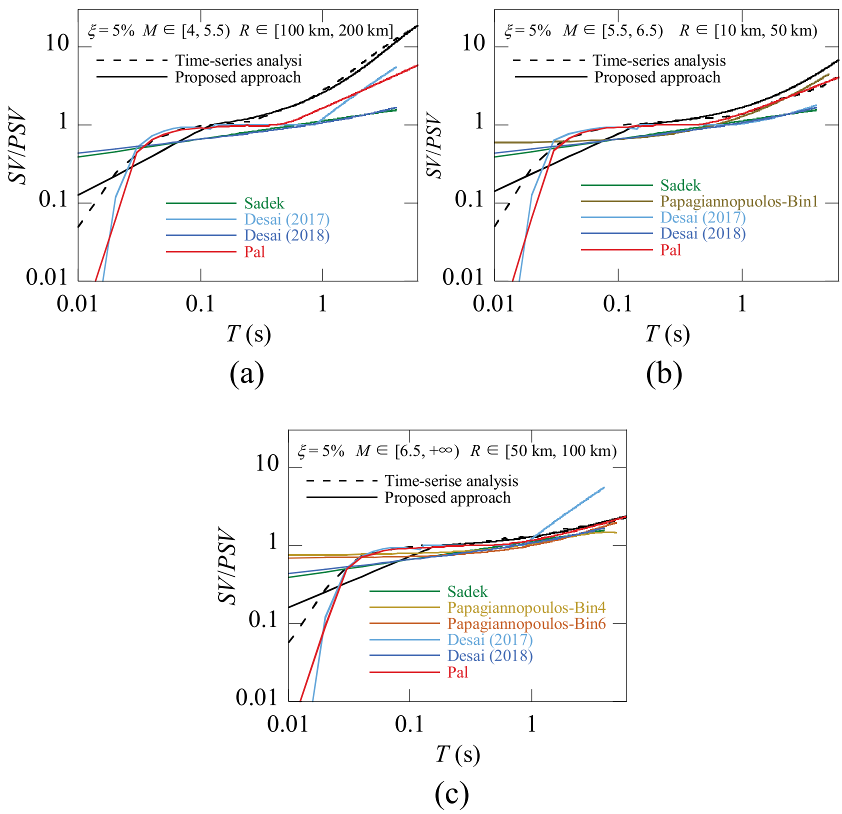

Figure 15. Comparison of the SV/PSV results obtained by the proposed and existing models considering a damping ratio of 5% in Class B for magnitudes of (a) $M \in [4, 5.5]$, (b) $M \in [5.5, 6.5]$, (c) $M \in [6.5, +\infty]$.

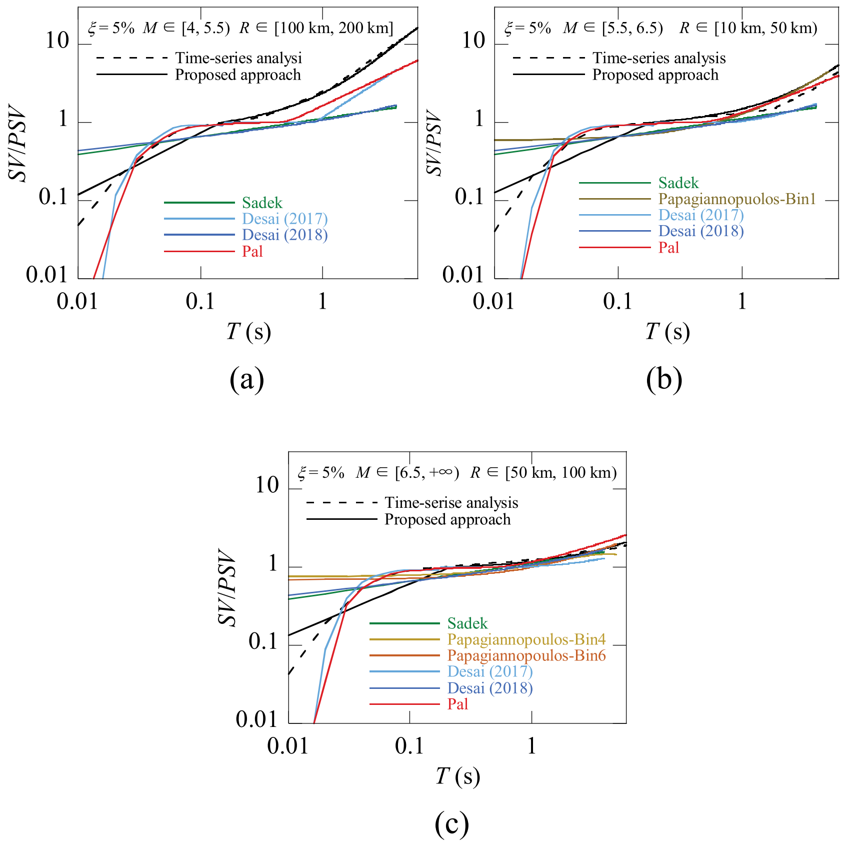

Figure 16. Comparison of the *SV/PSV* results obtained by the proposed and existing models considering a damping ratio of 5% in Class C for magnitudes of (a) $M \in [4, 5.5]$, (b) $M \in [5.5, 6.5]$, (c) $M \in [6.5, +\infty]$.

The accuracies of the *SV*/*PSV* results obtained by the model of Papagiannopoulos et al. (2013) are relatively poor. It can be found that Pal and Gupta's model (Pal and Gupta 2021) has the best performance among the existing models. Nevertheless, the proposed model performs better than Pal and Gupta's model (Pal and Gupta 2021), especially for cases of moderate magnitudes and long periods (Figs. 15–22a,b). In addition, the proposed model demonstrates broader applicability compared to Pal and Gupta's model (Pal and Gupta 2021), which is limited to damping ratios from 0% to 10%. In contrast, the proposed model covers damping ratios ranging from 5% to 50%. Moreover, the proposed model has fewer relative errors than Pal and Gupta's model for 55.6% cases in site class B, 66.7% cases in site class C, 77.8% cases in site class D, and 61.1% cases in site class E.

5. Conclusion

This study discussed the effects of magnitude, distance, and site class on the relationship between pseudo-velocity response spectrum (PSV) and velocity response spectrum (SV), and developed an *SV*/*PSV* model incorporating effects of magnitude, distance, and site class based on a large number of ground motion records (16,660 horizontal acceleration time histories) from Japan Strong Motion Network. The following are the conclusions of this paper.

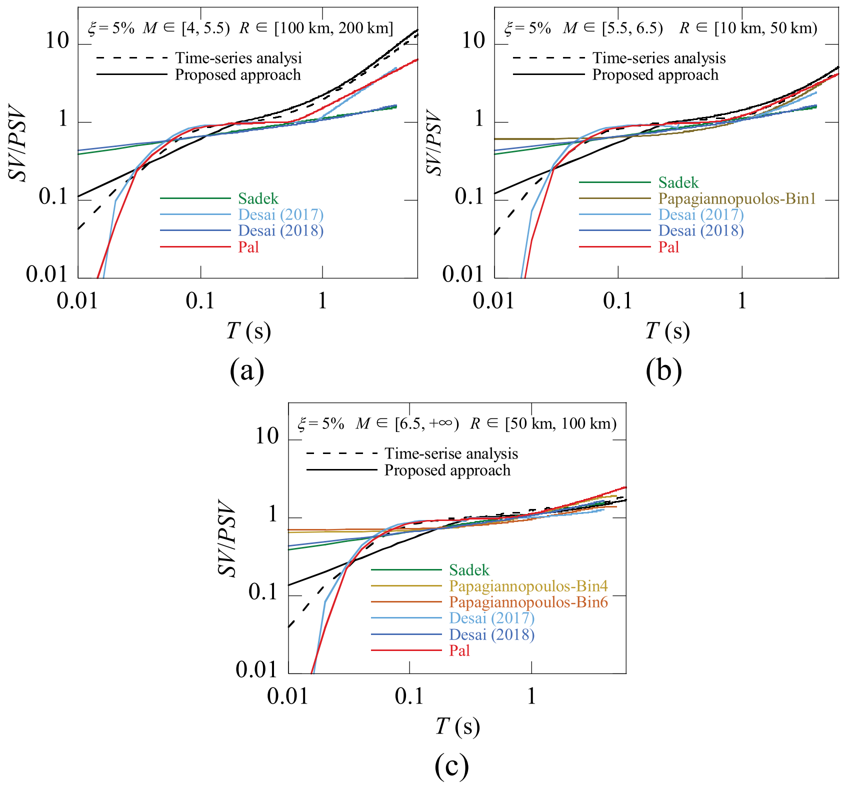

Figure 17. Comparison of the *SV/PSV* results obtained by the proposed and existing models considering a damping ratio of 5% in Class D for magnitudes of (a) $M \in [4, 5.5]$, (b) $M \in [5.5, 6.5]$, (c) $M \in [6.5, +\infty]$.

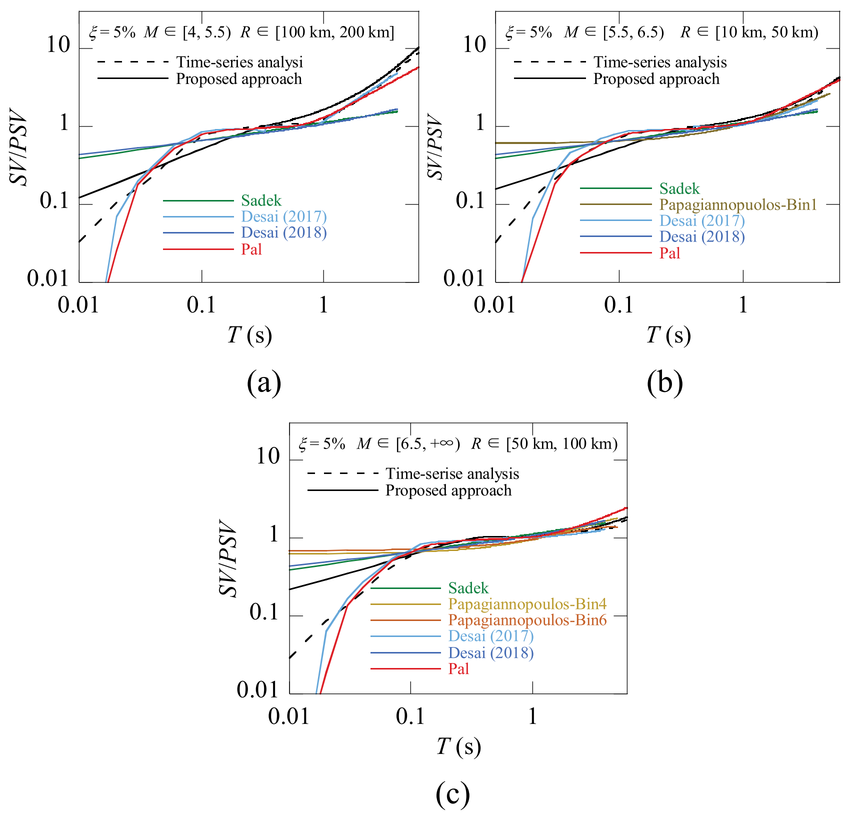

Figure 18. Comparison of the *SV/PSV* results obtained by the proposed and existing models considering a damping ratio of 5% in Class E for magnitudes of (a) $M \in [4, 5.5]$, (b) $M \in [5.5, 6.5]$, (c) $M \in [6.5, +\infty]$.

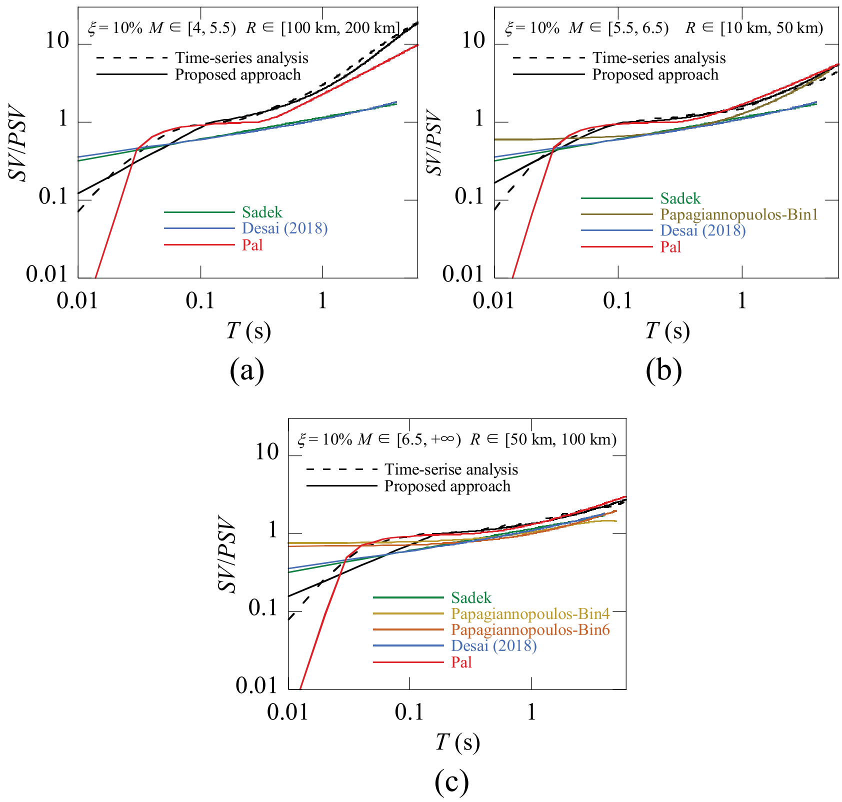

Figure 19. Comparison of the *SV/PSV* results obtained by the proposed and existing models considering a damping ratio of 10% in Class B for magnitudes of (a) $M \in [4, 5.5]$, (b) $M \in [5.5, 6.5]$, (c) $M \in [6.5, +\infty]$.

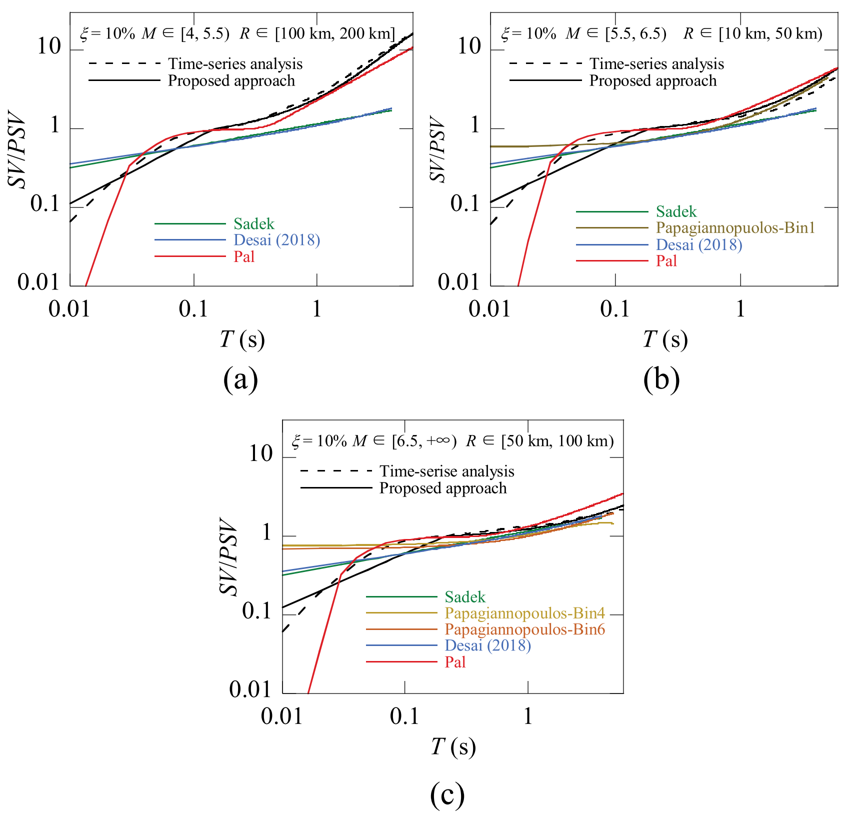

Figure 20. Comparison of the *SV/PSV* results obtained by the proposed and existing models considering a damping ratio of 10% in Class C for magnitudes of (a) $M \in [4, 5.5]$, (b) $M \in [5.5, 6.5]$, (c) $M \in [6.5, +\infty]$.

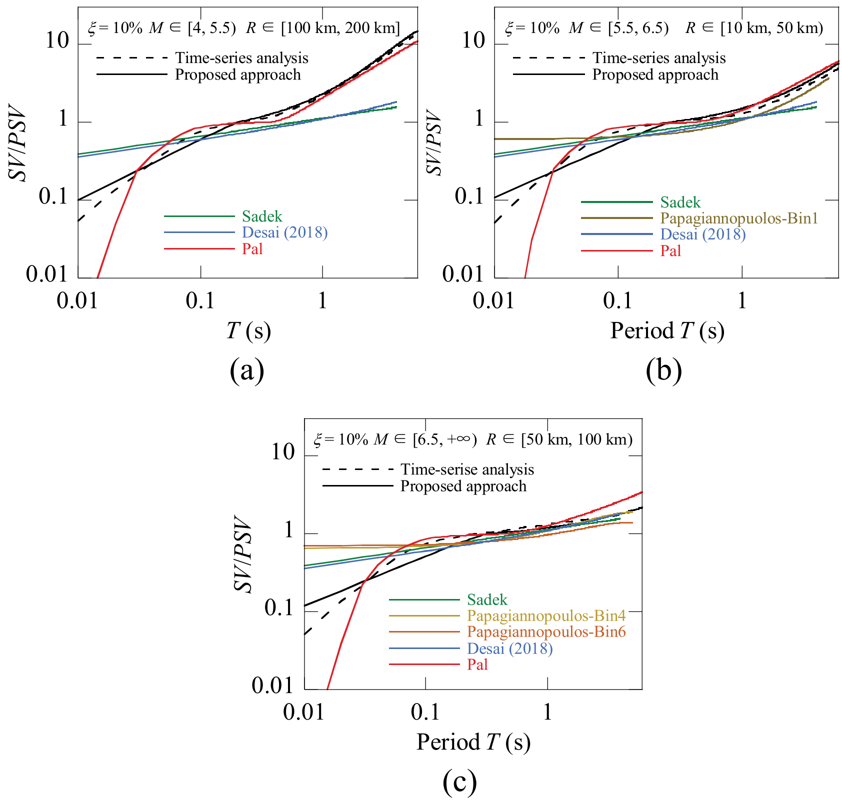

Figure 21. Comparison of the *SV/PSV* results obtained by the proposed and existing models considering a damping ratio of 10% in Class D for magnitudes of (a) $M \in [4, 5.5]$, (b) $M \in [5.5, 6.5]$, (c) $M \in [6.5, +\infty]$.

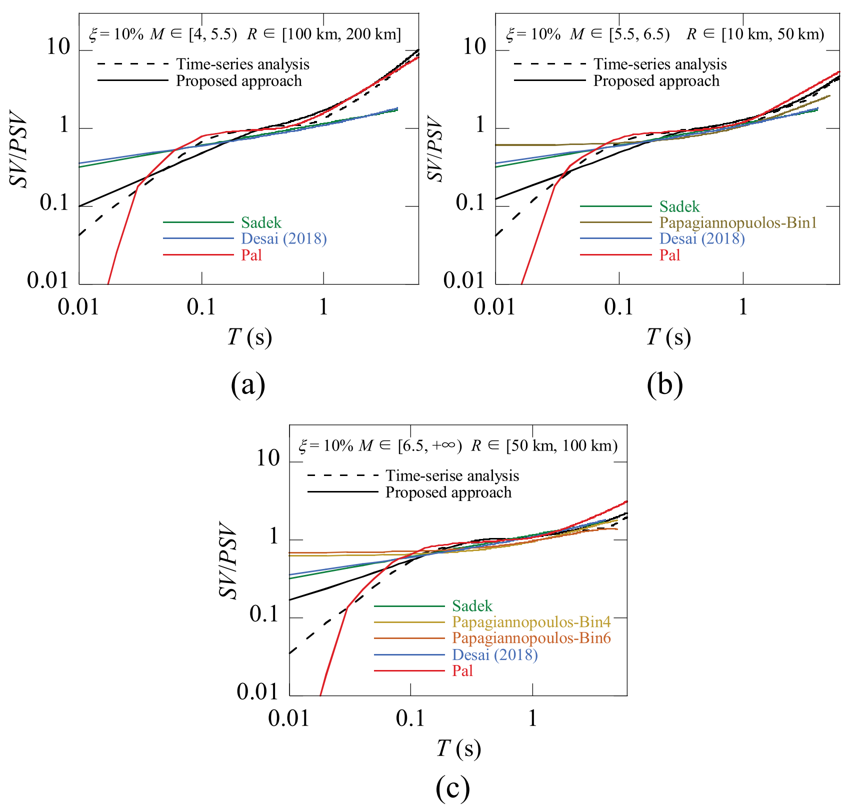

Figure 22. Comparison of the *SV/PSV* results obtained by the proposed and existing models considering a damping ratio of 10% in Class E for magnitudes of (a) $M \in [4, 5.5]$, (b) $M \in [5.5, 6.5]$, (c) $M \in [6.5, +\infty]$.

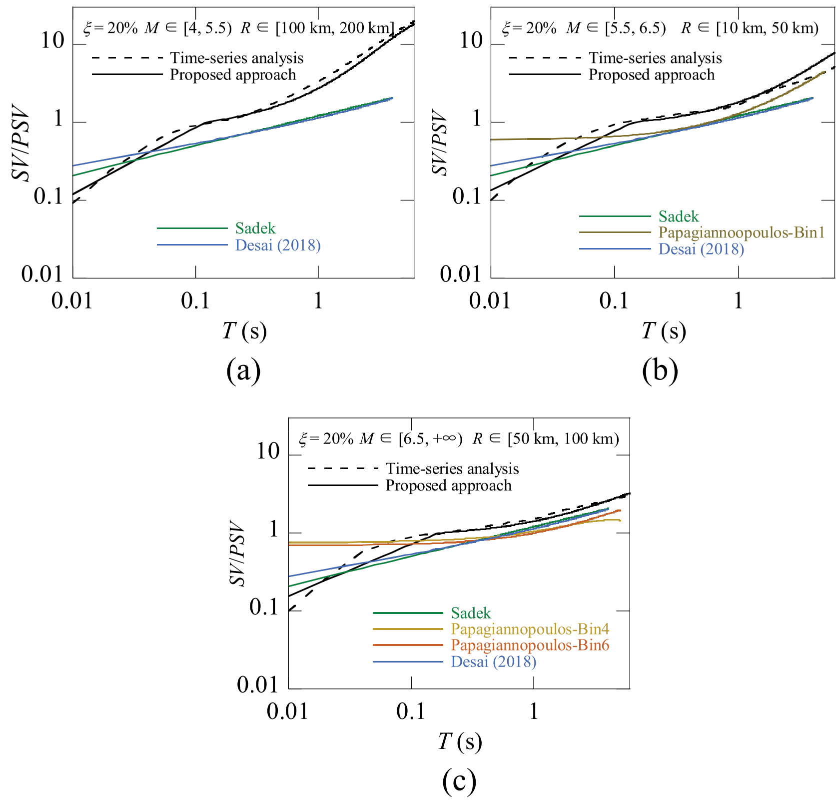

Figure 23. Comparison of the *SV*/*PSV* results obtained by the proposed and existing models considering a damping ratio of 20% in Class B for magnitudes of (a) $M \in [4, 5.5)$, (b) $M \in [5.5, 6.5)$, (c) $M \in [6.5, +\infty)$.

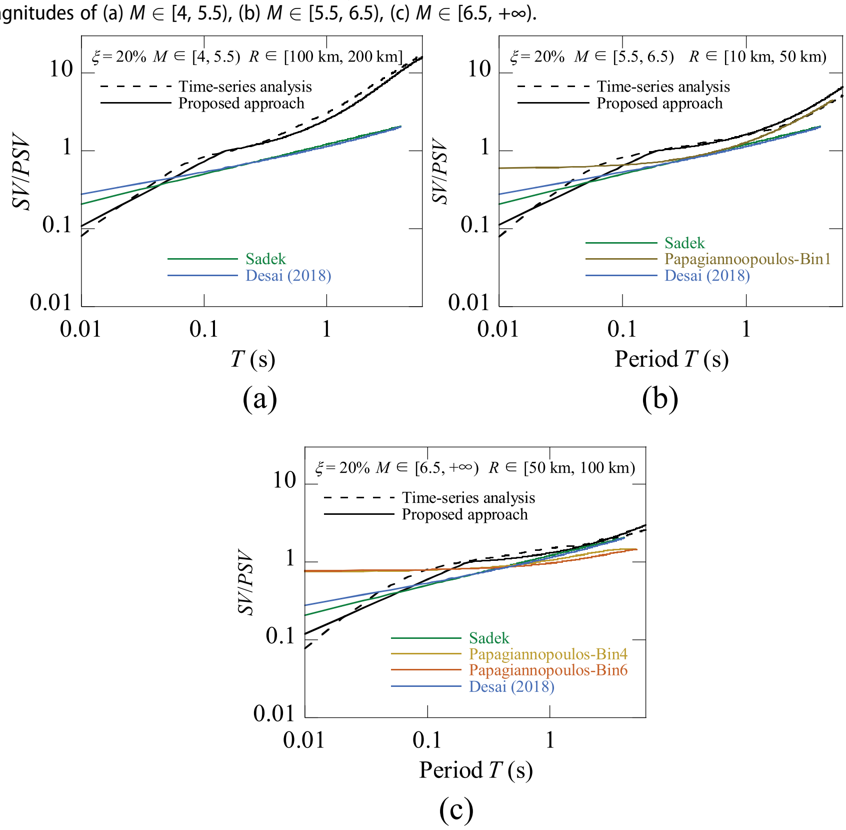

Figure 24. Comparison of the *SV*/*PSV* results obtained by the proposed and existing models considering a damping ratio of 20% in Class C for magnitudes of (a) $M \in [4, 5.5]$, (b) $M \in [5.5, 6.5]$, (c) $M \in [6.5, +\infty]$.

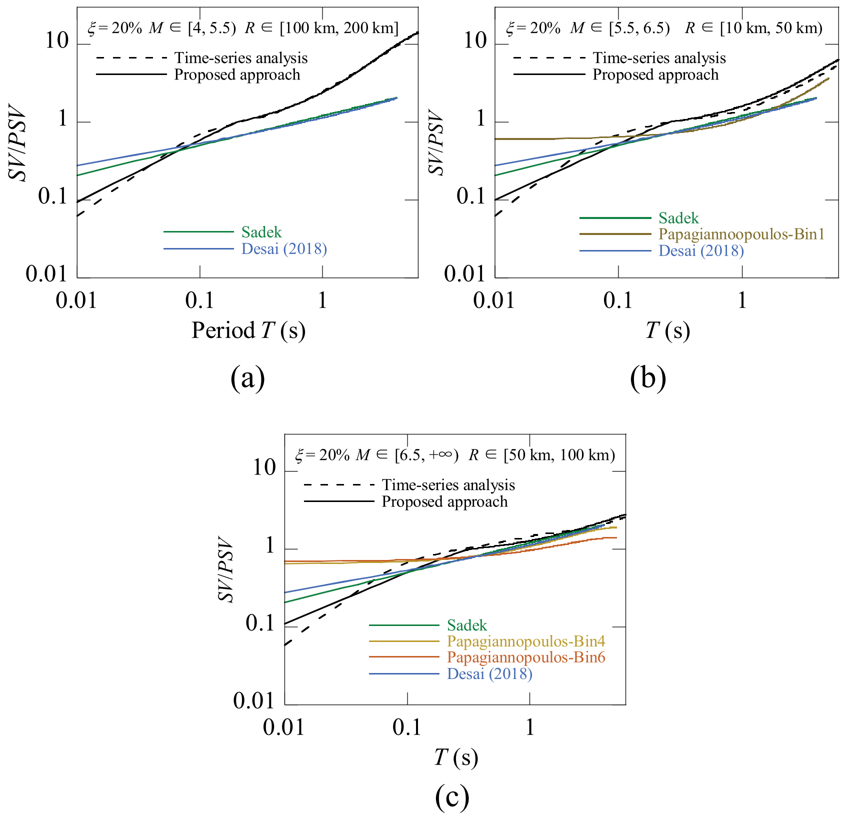

Figure 25. Comparison of the *SV/PSV* results obtained by the proposed and existing models considering a damping ratio of 20% in Class D for magnitudes of (a) $M \in [4, 5.5]$, (b) $M \in [5.5, 6.5]$, (c) $M \in [6.5, +\infty]$.

(1) The variation trends of the *SV*/*PSV* with the magnitude and distance are different at periods longer and shorter than the value corresponding to *SV*/*PSV* = 1. The *SV*/*PSV* decreases greatly with the magnitude over long periods, while the *SV*/*PSV* changes little with the magnitude in the short periods. At the long period range from 1 s to 6 s, the average value of *SV*/*PSV* decreases by 82%, for increasing magnitudes beyond 4. However, in the short period range between 0.01 and 0.1 s, the change is very small of the order of 2% only.
(2) The *SV*/*PSV* decreases with the distance in the short periods. In the long period range, the *SV*/*PSV* increases slightly with distance, while the degree of variation becomes very small as the site class changes from B to E. At longer periods, from 1 s to 6 s, the average value of *SV*/*PSV* increases by 29% for site class B and 8% for site class E, as the distance increases from [10 km, 50 km) to [100 km, 200 km].
(3) The average value of *SV*/*PSV* decreases gradually as the site class varies from B to E, it decreases by 55% at 0.01 — 0.1 s, while it decreases by 28% at 1— 6 s, for the cases with the magnitude of [6.5, +∞).
(4) The average value of *SV*/*PSV* increases with the damping ratio at long periods but decreases at the majority of short periods. However, the average value of *SV*/*PSV* becomes close between any two distinct dampings, as the damping increases beyond 30%.
(5) ln(s) increases with an increase in the magnitude and distance by analyzing the relationship between the response-spectrum-shape factor s and magnitude and distance. ln(s) is greatly affected by magnitude, while ln(s) is less affected by distance. Further, an expression for the relationship between parameter s and the magnitude and distance is established.

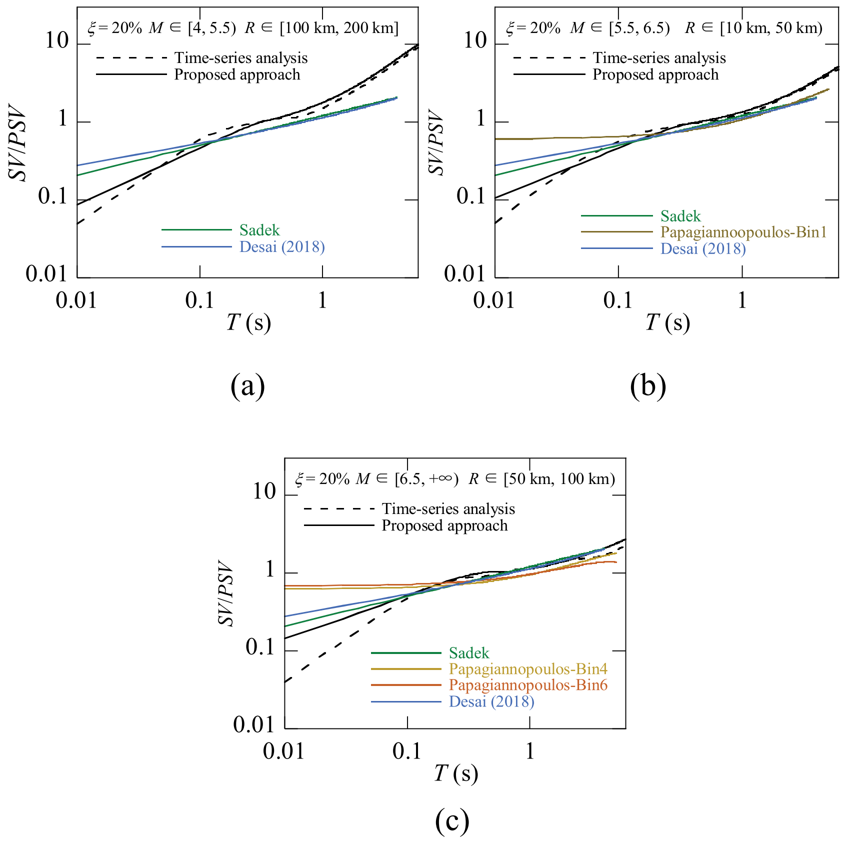

Figure 26. Comparison of the *SV*/*PSV* results obtained by the proposed and existing models considering a damping ratio of 20% in Class E for magnitudes of (a) $M \in [4, 5.5]$, (b) $M \in [5.5, 6.5]$, (c) $M \in [6.5, +\infty]$.

(6) The proposed *SV*/*PSV* model can be easily applied in seismic design by replacing magnitude and distance with the response-spectrum-shape factor *s*.
(7) The proposed *SV*/*PSV* model has good accuracy for most periods interested in the seismic design of structures, and the accuracy increases with the increase of the damping ratio.
(8) The proposed model outperformed the existing models in most cases and it demonstrates broader applicability compared to them, by covering damping ratios in the practical range of applications from 5% to 50%.

Acknowledgments

This study was partially supported by the National Natural Science Foundation of China. This study used strong-motion records from K-NET and KiK-net. The authors are grateful for the financial support and earthquake data.

Disclosure Statement

No potential conflict of interest was reported by the author(s).

Funding

This study was partially funded by the National Natural Science Foundation of China [Grant No. 52278135].

Author Contributions

Zheng Liu: Conceptualization, Methodology, Data curation, Writing -original draft, Investigation. Yan-gang Zhao: Visualization, Supervision, Writing – review & editing. Haizhong Zhang: Conceptualization, Data curation, Software, Visualization, Writing – review & editing, Supervision.

Code Availability

Available upon request.

Data Availability Statement

All data generated or analyzed during this study are included in this published article.

References

Andreotti, G., and G. M. Calvi. 2021. "Nonlinear Soil Effects on Observed and Simulated Response Spectra." *Earthquake Engineering and Structural Dynamics* 50 (14): 3831–3854. https://doi.org/10.1002/eqe.3535.

Aoi, S., T. Kunugi, H. Nakamura, and H. Fujiwara. 2011. "Deployment of New Strong Motion Seismographs of K-NET and KiK-Net." *Earthquake Data in Engineering Seismology, Geotechnical, Geological, and Earthquake Engineering* 14:167–186. https://doi.org/10.1007/978-94-007-0152-6_12.

Calvi, G. M., and G. Andreotti. 2022. "Effects of Local Soil, Magnitude and Distance on Empirical Response Spectra for Design." *Journal of Earthquake Engineering* 26 (3): 1117–1144. https://doi.org/10.1080/13632469.2019.1703847.

Castillo, T., and S. E. Ruiz. 2014. "Reduction Factors for Seismic Design Spectra for Structures with Viscous Energy Dampers." *Journal of Earthquake Engineering* 18 (3): 323–349. https://doi.org/10.1080/13632469.2013.860932.

Desai, R. S., and S. N. Tande. 2017. "Estimation of Spectral Velocity at Long Periods for Application in Velocity Dependent Seismic Energy Management Devices." *Journal of Structural Engineering* 44 (1): 14–22.

Desai, R. S., and S. N. Tande. 2018. "Estimate of Peak Relative Velocity from Conventional Spectral Velocity for Response Spectrum Based Force Evaluation in Damping Devices." *Structures* 15:378–387. https://doi.org/10.1016/j.istruc.2018.07.014.

Federal Emergency Dissipation Agency (FEMA-450). 2003. *NEHRP Recommended Provisions for Seismic Regulations for New Buildings and Other Structures. Part 1: Provisions and Part 2: Commentary*. Washington, DC: FEMA P-2082-1.

Gupta, V. K. 2009. "A New Approximation for Spectral Velocity Ordinates at Short Periods." *Earthquake Engineering and Structural Dynamics* 38 (7): 941–949. https://doi.org/10.1002/eqe.877.

Gupta, V. K., and M. D. Trifunac. 1990. "Response of Multistoried Buildings to Ground Translation and Rocking During Earthquakes." *Probabilistic Engineering Mechanics* 5 (3): 138–145. https://doi.org/10.1016/0266-8920(90)90005-5.

Hang, B. J., H. Z. Zhang, and Y. G. Zhao. 2022. "Effects of Magnitude, Epicentral Distance and Site Class on the Relationship Between Spectral and Pseudo-Spectral Acceleration." *Earthquake Engineering and Engineering Dynamics* 42 (4): 219–228. (In Chinese).

Kanno, T., A. Narita, N. Morikawa, H. Fujiwara, and Y. Fukushima. 2006. "A New Attenuation Relation for Strong Ground Motion in Japan Based on Recorded Data." *Bulletin of the Seismological Society of America* 96 (3): 879–897. https://doi.org/10.1785/0120050138.

Kumari, R., and V. K. Gupta. 2007. "A Modal Combination Rule for Peak Floor Accelerations in Multistoried Buildings." *ISET Journal of Earthquake Technology* 44 (1): 213–231.

National Earthquake Hazards Reduction Program. 2000. "Recommended Provisions for Seismic Regulations for New Buildings and Other Structures." In *Federal Emergency Management Agency*. Washington, DC.

National Research Institute for Earth Science and Disaster Resilience. 1995. Strong-Motion Seismograph Networks (K-NET, KIK-net).

Okada, Y., K. Kasahara, S. Hori, K. Obara, S. Sekiguchi, H. Fujiwara, A. Yamamoto. 2004. "Recent Progress of Seismic Observation Networks in Japan—Hi-net, F-Net, K-NET and KiK-net—." *Earth, Planets and Space* 56 (8): xv–xxviii. https://doi.org/10.1186/BF03353076.

Pal, A., and V. K. Gupta. 2021. "A Note on Spectral Velocity Approximation at Shorter Intermediate Periods." *Soil Dynamics and Earthquake Engineering* 141:106422. https://doi.org/10.1016/j.soildyn.2020.106422.

Papagiannopoulos, G. A., G. D. Hatzigeorgiou, and D. E. Beskos. 2013. "Recovery of Spectral Absolute Acceleration and Spectral Relative Velocity from Their Pseudo-Spectral Counterparts." *Earthquake and Structures* 4 (5): 489–508. https://doi.org/10.12989/eas.2013.4.5.489.

Rathje, E. M., F. Faraj, S. Russell, and J. D. Bray. 2004. "Empirical Relationships for Frequency Content Parameters of Earthquake Ground Motions." *Earthquake Spectra* 20 (1): 119–144. https://doi.org/10.1193/1.1643356.

Sadek, F., B. Mohraz, and M. A. Riley. 2000. "Linear Procedures for Structures with Velocity-Dependent Dampers." *Journal of Structural Engineering* 126 (8): 887–895. https://doi.org/10.1061/(ASCE)0733-9445(2000)126:8(887).

Sadhu, A., and V. K. Gupta. 2008. "A Modal Combination Rule for Ordered Peak Response Under Multi-component Ground Motion." *ISET Journal of Earthquake Technology* 45 (3/4): 79–96.

Samdaria, N., and V. K. Gupta. 2018. "A New Model for Spectral Velocity Ordinates at Long Periods." *Earthquake Engineering and Structural Dynamics* 47 (1): 169–194. https://doi.org/10.1002/eqe.2945.

Santos-Santiago, M. A., S. E. Ruiz, and F. Valenzuela-Beltrán. 2022. "Influence of Higher Modes of Vibration on the Seismic Response of Buildings with Linear and Nonlinear Viscous Dampers." *Journal of Earthquake Engineering* 26 (8): 3914–3937. https://doi.org/10.1080/13632469.2020.1822223.

Trifunac, M. D., and V. K. Gupta. 1991. "Pseudorelative Acceleration Spectrum." *Journal of Engineering Mechanics* 117 (4): 924–927. https://doi.org/10.1061/(ASCE)0733-9399(1991)117:4(924).

Zhang, H. Z., J. Deng, and Y. G. Zhao. 2023. "Damping Modification Factor of Pseudo-acceleration Spectrum Considering Influences of Magnitude, Distance and Site Conditions." *Earthquakes and Structures* 25 (5): 325–342. https://doi.org/10.12989/eas.2023.25.5.325.

Zhang, H. Z., and Y. G. Zhao. 2021. "Effects of Earthquake Magnitude, Distance, and Site Conditions on Spectral and Pseudospectral Velocity Relationship." *Bulletin of the Seismological Society of America* 111 (6): 3160–3174. https://doi.org/10.1785/012021015.

Zhang, H. Z., and Y. G. Zhao. 2022. "Damping Modification Factor of Acceleration Response Spectrum Considering Seismological Effects." *Journal of Earthquake Engineering* 26 (16): 8359–8382. https://doi.org/10.1080/13632469.2021.1991521.

Zhang, H. Z., Y. G. Zhao, F. W. Ge, Y. C. Fang, and T. Ochiai. 2023. "Estimation of input energy spectrum from pseudo-velocity response spectrum incorporating the influences of magnitude, distance, and site conditions." *Engineering Structures* 274 (1): 115165. https://doi.org/10.1016/j.engstruct.2022.115165.

Zuccolo, E., G. Andreotti, and G. M. Calvi. 2023. "PSHA-Based Design Spectrum: An Application of the Design Spectrum Predictive Model for Seismic Regulation Purposes." *Journal of Earthquake Engineering* 27 (15): 4494–4511. https://doi.org/10.1080/13632469.2023.2171162.

Appendix A

SV	Velocity response spectrum	$C(T)$	Transition curve of the short periods
PSV	Pseudo-velocity response spectrum	$T_{\lim}$	Limiting period significantly longer than T_c
PSA	Pseudo-acceleration response spectrum	w_0–w_6	Regression coefficients of Eq. (6a)
s	Response-spectrum-shape factor	T_{PSA}	Period at which the PSA is maximum
SD	Displacement response spectrum	T_{PSV}	Period at which the PSV is maximum
T	Natural structural period	r	Solution coefficient of Eq. (6b)
ξ	Damping ratio	$PSA_{\lim}$	Value of PSA corresponding to the period $T_{\lim}$
q_1–q_4	Regression coefficients of Eq. (2)	u_1–u_4	Regression coefficients of Eq. (7)
T_c	Mean period of the base acceleration corresponding to the centroid of its Fourier spectrum	T_s	Dominant period
PGA	Peak ground acceleration	k_1–k_{12}	Regression coefficients of Eqs. (8 and 9)
C_n	Fourier amplitudes of ground motion	M	Magnitude
f_n	Discrete frequencies	R	Distance
$\bar{T}$	Period corresponding to the centroid of the spectral displacement (SD) curve.	$\bar{v}_{s30}$	Shear-wave velocity in the upper 30 m
$T_{\max}$	End of the velocity-sensitive region in the response spectrum of the ground motion	$\bar{v}_{s20}$	Shear-wave velocity in the upper 20 m
l	Change speed of the PSV deviating from the SV as T increases	SA	Acceleration response spectrum
o_1–o_4	Regression coefficients of Eq. (5a,b)	a_1–a_4	Regression coefficients of Eq. (11)
p	Regression coefficient of Eq. (5b)	T_0	Period corresponding to $SV/PSV = 1$
T_{end}	End of the velocity-sensitive region in the response spectrum	$PSA(6s)$	Value of PSA at 6s
$PSA(T_{\mathrm{end}})$	Value of PSA corresponding to the period T_{end}	m_1, m_1, m_3, n_1, and n_2	Regression coefficients of Eq. (12)
$PSA(T_{\max})$	Value of PSA corresponding to the period $T_{\max}$	b_1, b_2, b_3, c_1, c_2, c_3, d_1, d_2, d_3, e_1, e_2, and e_3	Regression coefficients of Eqs. (13–16)